Hamiltonian strong-coupling expansions for (2+1)-dimensional quantum electrodynamics

C. J. Burden* and C. J. Hamer†
Department of Theoretical Physics, Research School of Physical Sciences, Australian National University, G.P.O. Box 4, Canberra, Australian Capital Territory 2601, Australia
(Received 1 May 1987; revised manuscript received 26 August 1987)

Linked cluster expansions are applied to calculate strong-coupling series for lattice quantum electrodynamics in $(2+1)$ dimensions. Series expansions are calculated for the ground-state energy and chiral condensate to $O(g^{-32})$ in the dimensionless coupling and for the symmetric and antisymmetric "photon-ball" mass gaps to $O(g^{-16})$ for various values of the fermion mass. The series do not extend well enough into the weak-coupling regime to allow an accurate matching with the expected weak-coupling behavior, though the correct qualitative behavior is observed for the ground-state energy and chiral condensate.

I. INTRODUCTION

A major problem facing lattice gauge theory at present is how to deal with dynamical fermions. Following the success of Monte Carlo algorithms in the quenched approximation, the main thrust so far has been towards extending the Monte Carlo method. Some limited success has been obtained, though the methods tend to be expensive in computer time, generally requiring the power of an array processor. A possible alternative is to revive the Hamiltonian formalism of Kogut, Susskind, and co-workers.[1,2] In the past, Hamiltonian strong-coupling expansions have been largely neglected; the early hand calculations for QCD quickly became impractical due to the rapid proliferation of diagrams. However, the subsequent development of linked cluster expansions,[3,4] making it possible to automate the procedure in the computer, has rekindled some interest in strong-coupling expansions.

To date, linked cluster expansions have been applied with varying degrees of success to pure gauge theories in $(2+1)$ and $(3+1)$ dimensions.[4-6] More recently, matter fields have been included in a study of the Z_2 Abelian Higgs model in $(2+1)$ dimensions.[7] This paper is a first attempt to extend the method of cluster expansions to include fermions. As a test case, we have chosen to study quantum electrodynamics in $(2+1)$ dimensions. This is the simplest confining lattice theory with independent gauge field degrees of freedom, and dynamical fermions. To describe the fermions, we use the four-component spinor theory of Pisarski,[8] since four-component spinors arise naturally as a consequence of fermion doubling on the lattice in $(2+1)$ dimensions.[9] The theory has important qualitative features in common with $(3+1)$-dimensional QCD: it is believed to be confining at large distances, while in the massless limit it displays a chiral-like symmetry which is thought to be spontaneously broken.[8,10] It is a super-renormalizable theory,[11] so that we may expect simple dimensional scaling of physical quantities in the continuum limit, as functions of either the bare fermion mass or the coupling constant.

In this paper we generate strong-coupling series expansions for the ground-state energy and chiral condensate to $O(g^{-32})$ and for the "photon-ball" mass to $O(g^{-16})$. We find, unfortunately, that approximants to these series do not converge well in the weak-coupling regime, and that we are unable to make reliable extrapolations to the continuum limit. Without some further technical breakthrough, it seems unlikely that strong-coupling series expansions will be very useful in the treatment of dynamical fermions in QCD.

The layout of the paper is as follows: The Hamiltonian formalism of $(2+1)$-dimensional QED is summarized in the next section, while details of the cluster expansion method are given in Sec. III. Section IV is devoted to an analysis of our series expansions. In Sec. V we examine potential improvements as more terms are added to the series expansions, and our conclusions are summarized in Sec. VI.

II. (2+1)-DIMENSIONAL LATTICE QED

While Hamiltonian lattice gauge theory has been established for some time, there seems to be practically no application in the literature to gauge theories with fermions in an odd number of space-time dimensions. The only case known to the authors is a paper by Semenoff[12] dealing with valence electrons in an hexagonal graphite lattice. This section is therefore devoted to a summary of the $(2+1)$-dimensional lattice Hamiltonian.

We begin with the Hamiltonian

$$H=\frac{g^2}{2a}W\ , \tag{1a}$$

$$W=W_0+yW_1+y^2W_2\quad (y=1/g^2)\ , \tag{1b}$$

$$W_0=W_e+W_\mu=\sum_l E_l{}^2+\mu\sum_r(-1)^{r_1+r_2}\chi^\dagger(r)\chi(r)\ , \tag{1c}$$

$$W_1=\sum_{r,i}\eta_i(r)[\chi^\dagger(r)U_i(r)\chi(r+a\hat{i})+\text{H.c}]\ ,$$
$$\eta_1(r)=(-1)^{r_2+1},\quad \eta_2(r)=1\ , \tag{1d}$$

$$W_2=-\sum_p(U_{\partial p}+U_{\partial p}^\dagger)\ , \tag{1e}$$

where $r=(r_1,r_2)$ labels the sites, l the links, p the plaquettes and $i=1,2$ the directions on a square two-dimensional spatial lattice with spacing a. The dimensionless coupling g and dimensionless fermion mass μ are defined in terms of their continuum counterparts e and m by

$$g^2=e^2a, \quad \mu=\frac{2am}{g^2} . \tag{2}$$

The bosonic operators E, U and single-component-per-site fermion operators χ satisfy

$$\begin{aligned} &[E_l,U_{l'}]=U_l\delta_{ll'} , \\ &[E_l,U_{l'}^\dagger]=-U_l^\dagger\delta_{ll'} , \\ &\{\chi^\dagger(r),\chi(r')\}=\delta_{rr'} , \\ &[E_l,\chi(r)]=[E_l,\chi^\dagger(r)]=[U_l,\chi(r)]=[U_l,\chi^\dagger(r)]=0 . \end{aligned} \tag{3}$$

$U_{\partial p}$ means the product

$$U_1(r)U_2(r+a\hat{1})U_1^\dagger(r+a\hat{2})U_2^\dagger(r)$$

around the plaquette p.

In the naive continuum limit, Eq. (1) becomes the $(2+1)$-dimensional QED Hamiltonian

$$\int d^2x[\tfrac{1}{2}(\mathbf{E}_{\rm cont}{}^2+B^2)-i\psi^\dagger\boldsymbol{\alpha}\cdot(\boldsymbol{\nabla}+ie\,\mathbf{A})\psi+m\psi^\dagger\gamma_0\psi] , \tag{4}$$

where ψ is a single four-component Dirac spinor[8] and $\alpha_i=\gamma_0\gamma_i$, with γ_0, γ_1, and γ_2 4×4 Dirac matrices. The pure gauge part is easily obtained from the appropriate terms in (1) using the replacements $E_l\to ae^{-1}E^i_{\rm cont}(r)$ and $U_l=\exp[iea\,A_i(r)]$. The fermion part involves Kogut-Susskind staggered fermions. Consider the pure fermion Hamiltonian

$$H_f=\frac{1}{2a}\sum_{i,r}\eta_i(r)[\chi^\dagger(r)\chi(r+a\hat{i})+\chi^\dagger(r+a\hat{i})\chi(r)] +m\sum_r(-1)^r\chi^\dagger(r)\chi(r) . \tag{5}$$

Following Susskind[13] we define

$$\xi(r)=i^r\chi(r) ,$$

and further define $\xi_1,\ldots,\xi_4$ to be equal to ξ on the respective sublattices of Fig. 1, and zero otherwise. The first term in the Hamiltonian (5) becomes

$$H_f^{\rm kin}=-i\sum_r(\xi_1^\dagger\xi_2^\dagger\xi_3^\dagger\xi_4^\dagger)\begin{pmatrix}0&-\Delta_1&0&\Delta_2\\-\Delta_1&0&\Delta_2&0\\0&\Delta_2&0&\Delta_1\\\Delta_2&0&\Delta_1&0\end{pmatrix}\begin{pmatrix}\xi_1\\\xi_2\\\xi_3\\\xi_4\end{pmatrix} ,$$

where

$$\Delta_i\xi_k(r)=[\xi_k(r+a\hat{i})-\xi_k(r-a\hat{i})]/2a .$$

Now introducing a four-component spinor field $\psi(R)$ on a lattice of spacing $2a$:

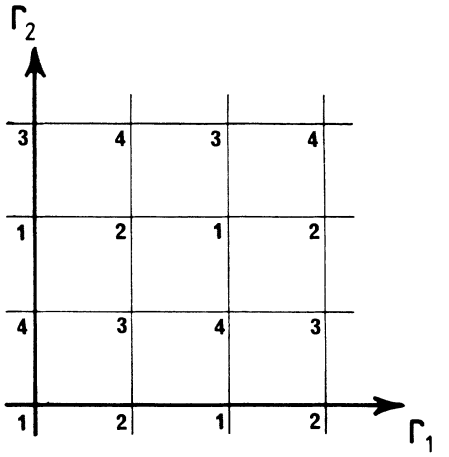

FIG. 1. Sublattices supporting the staggered fermion fields $\xi_1,\ldots,\xi_4$.

$$\begin{pmatrix}\psi_1\\\psi_2\\\psi_3\\\psi_4\end{pmatrix}=\frac{1}{2\sqrt{2}a}\begin{pmatrix}0&-i&0&1\\1&0&-i&0\\-i&0&1&0\\0&1&0&-i\end{pmatrix}\begin{pmatrix}\xi_1\\\xi_2\\\xi_3\\\xi_4\end{pmatrix} , \tag{6}$$

where $r_i=2R_i$ or $2R_i+1$ for r_i even or odd, respectively, we obtain

$$H_f=-4a^2i\sum_R\psi^\dagger(\alpha_1\Delta_1+\alpha_2\Delta_2)\psi . \tag{7}$$

In obtaining Eq. (7) we have used the Dirac representation

$$\gamma_0=\begin{pmatrix}\sigma_3&\\&-\sigma_3\end{pmatrix}, \quad \gamma_1=i\begin{pmatrix}\sigma_1&\\&-\sigma_1\end{pmatrix} , \quad \gamma_2=i\begin{pmatrix}\sigma_2&\\&-\sigma_2\end{pmatrix} .$$

Since the fields are defined on sublattices of spacing $2a$, we use the replacement $4a^2\sum_R\to\int d^2x$ to retrieve the kinetic term in the continuum Hamiltonian (4). The mass term is obtained in a similar way. An equivalent continuum limit in terms of two flavors of two-component spinors of opposite mass was obtained by Semenoff[12] for the hexagonal lattice, while the equivalent Lagrangian formalism is dealt with in Ref. 9.

The continuum four-component Dirac Hamiltonian (4) enjoys a global U(2) "chiral" symmetry in the zero-mass limit.[8,10] The Lie algebra of this symmetry is spanned by the 4×4 matrices:

$$I,\ \gamma_4=\begin{pmatrix}0&I\\I&0\end{pmatrix}, \quad \gamma_5=\begin{pmatrix}0&-iI\\iI&0\end{pmatrix} ,$$

and

$$\gamma_{45}=-i\gamma_4\gamma_5 .$$

As in the $(3+1)$-dimensional case,[13] the lattice breaks this down to a discrete symmetry generated by shifts of one lattice spacing. The x and y shifts defined by

$$\chi(r)\to\chi^{(X)}(r)=-\chi(r+a\hat{1}) ,$$
$$\chi(r)\to\chi^{(Y)}(r)=(-1)^{r_1}\chi(r+a\hat{2}) \tag{8}$$

leave the kinetic term in the Hamiltonian (5) invariant, but not the mass term. The corresponding continuum field transformations, obtained by a straightforward application of (6), are

$$\psi\to\psi^{(X)}=i\gamma_4\psi=e^{i(\pi/2)\gamma_4}\psi ,$$
$$\psi\to\psi^{(Y)}=i\gamma_5\psi=e^{i(\pi/2)\gamma_5}\psi .$$

Clearly, composing both shifts to produce a shift along the lattice diagonal gives a discrete γ_{45} rotation in the continuum fields.

Pisarski[8] and others[10,14] have studied the large-N_{flavor} limit of continuum QED in $(2+1)$ dimensions. Their analyses of the Schwinger-Dyson equations show a dynamical breakdown of chiral symmetry. In the lattice Hamiltonian formalism this should show up as a nonzero value of the chiral condensate $(2a)^{-2}\sum_r(-1)^r\chi^\dagger(r)\chi(r)$ per unit lattice site as the continuum limit is approached.

The Hamiltonian (1) acts on a Fock space spanned by the usual strong-coupling basis. With each link is associated an integer flux $|n_l\rangle$ such that $E_l|n_l\rangle=n_l|n_l\rangle$. The operators U_l and $U_l^\dagger$ increase and decrease the flux on link l by one unit, respectively. Each site of the lattice can be in one of two states $|+\rangle$ or $|-\rangle$ satisfying

$$\chi^\dagger|-\rangle=|+\rangle,\quad \chi^\dagger|+\rangle=0 ,$$
$$\chi|-\rangle=0,\quad \chi|+\rangle=|-\rangle .$$

We consider first the strong-coupling expansion of the massless theory ($\mu=0$). To zeroth order in the expansion variable y, only W_e is important. The zeroth-order ground state is highly degenerate, having flux $n_l=0$ on each link, while the fermionic site states are totally arbitrary. This arbitrariness is broken down at the next order by the kinetic term Eq. (1d) to two states $|A\rangle$ and $|B\rangle$ whose fermionic content is defined by

$$|A\rangle=\begin{cases}|+\rangle & \text{on odd sites} ,\\ |-\rangle & \text{on even sites} ,\end{cases}$$
$$|B\rangle=\begin{cases}|-\rangle & \text{on odd sites} ,\\ |+\rangle & \text{on even sites} .\end{cases} \tag{9}$$

("Odd" and "even" refer to the sign of r_1+r_2.) The chiral shifts (8) clearly map these states into each other. When the mass term W_μ is included, chiral symmetry is explicitly broken and state $|A\rangle$ is energetically favored. In the following analysis we shall take $|A\rangle$ as the unperturbed strong-coupling ground state for both the massive and massless theories. This is interpreted as the state with no fermions present. When the sign on a particular even (odd) site differs from the sign in the unperturbed site, the site is occupied by a positively (negatively) charged fermion. The exclusion principle prohibits more than one fermion occupying any site.

The first-order perturbation W_1 creates or destroys an electron-positron pair on neighboring sites joined by a link of flux. Applying W_1 to a particular link only gives a nonzero state if the sites at the ends of the links are either both empty or both occupied by fermions. The second-order perturbation W_2 creates or destroys a plaquette of flux. Gauge invariance ensures that, for any state produced from the unperturbed vacuum by application of W_1 and W_2, the net flux from any site is equal to the charge of the fermion at that site.

III. LINKED CLUSTER EXPANSIONS

The strong-coupling expansion of any physical quantity now proceeds via Rayleigh-Schrödinger perturbation theory. Each term in the series can be envisaged as a set of diagrams.[1,2] the physical extent of the diagrams across the lattice increasing with the order of perturbation theory. It is this property of the diagrammatic expansion that allows the procedure to be handled numerically via linked cluster expansions. This method was proposed by Nickel[3] and applied successfully to Z_2 and U(1) pure gauge models by Hamer and Irving.[4,5]

A. Ground-state energy

The simplest application of the linked cluster method is to the series expansion for the ground-state energy $\omega_0(y)$. The proof of the validity of the method when fermions are present is much the same as for the pure gauge case, and the reader is referred to Ref. 4 for details. The main ingredients of the argument run as follows. The series expansion of $\omega_0(y)$ to order y^{2N} can be decomposed as a sum over a particular finite set of connected sublattices or clusters:

$$\omega_0(y)=\sum_\alpha l_a\epsilon_\alpha^{(2N)}(y)+O(y^{2N+2}) . \tag{10}$$

The number l_α is the lattice constant for the cluster α, that is, the number of ways α can be embedded in the infinite lattice per unit site. The set of clusters involved in Eq. (10) is determined by the extent of the connected diagrams occurring in the Rayleigh-Schrödinger expansion of the dimensionless Hamiltonian W [Eq. (1b)]. We define a connected cluster α to have order $\mathcal{O}(\alpha)=N$ if the first diagram in the perturbation expansion to span the cluster occurs at order y^{2N} (see Fig. 2). Since the first-order perturbation W_1 and second-order perturbation W_2 involve links and plaquettes, respectively, a lower bound on $\mathcal{O}(\alpha)$ is given by

$$\mathcal{O}(\alpha)\geq 2n_p(\alpha)+n_l(\alpha) , \tag{11}$$

where n_p is the number of plaquettes in α, and n_l the number of links not contained in plaquettes (see Fig. 3). The sum in Eq. (10) is over all clusters α with $\mathcal{O}(\alpha)\leq N$.

The quantities $\epsilon_\alpha^{(2N)}(y)$ in Eq. (10) are polynomials of degree $2N$ representing the contributions to the ground-state energy series expansion from diagrams spanning the cluster α. They are evaluated from the result analogous to (10) for a finite cluster:

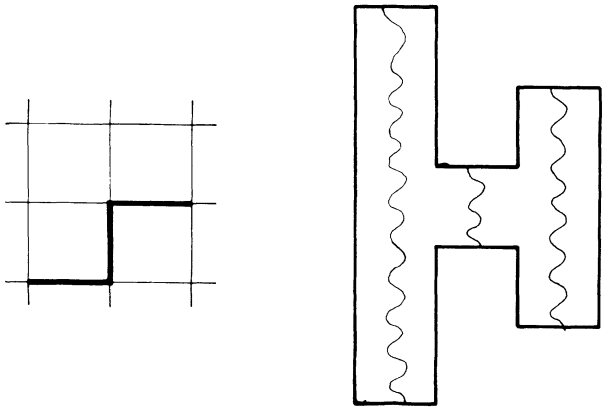

FIG. 2. A cluster of order 3 and the order-y^6 diagram spanning it arising from the term $\langle 0 | W_1[(P_0/E_0 - W_0)W_1]^3 | 0 \rangle$ in the perturbation expansion.

$$E_\alpha^{(2N)} = \sum_\beta C_\beta^\alpha \epsilon_\alpha^{(2N)} . \tag{12}$$

The sum is over the subclusters β which embed into α (including α itself), while C_β^α is the (weak) embedding constant of β in α (Ref. 15), that is, the number of ways cluster β can be embedded in cluster α. $E_\alpha^{(2N)}$ is the ground-state energy of the Hamiltonian W restricted to the cluster α evaluated to order $2N$. For the minimal one-link cluster ($\alpha=1$, say) we define $\epsilon_1^{(2N)} = E_1^{(2N)}$.

Algorithms for generating clusters and their embedding and lattice constants exist[16] and can be adapted to handle a search for all clusters satisfying the cutoff (11). We used a tree search which at each stage added new links or plaquettes to sites of clusters in the existing list to generate new clusters. Having generated a list of clusters and embedding constants, we employed a modified version of an algorithm due to Hornby and Barber[17] to obtain a series expansion for $E_\alpha^{(2N)}$ on each cluster. The $\epsilon_\alpha^{(2N)}$'s are then calculated iteratively from (12), and finally substituted into the formula (10) to produce the required result.

A couple of remarks regarding the set of clusters are in order. First, we note that the above algorithm is not invalidated if the cluster list contains unnecessary clusters. The algorithm will automatically give $\epsilon_\alpha^{(2N)} = 0$ for any cluster with $\mathcal{O}(\alpha) > N$. However, it is in the interests of efficiency both in computer time and in reducing roundoff errors to make the cutoff as low as possible, especially since it is the larger clusters which are most expensive in computer time. It turns out that the cutoff (11) is particularly conservative and contains many clusters which are effectively disconnected at order N. This is because the operator W_2 acting on a plaquette p does not feel the action of the link operator W_1 sharing only one site in common with p, and may see the link as being disconnected from the plaquette. We have therefore been able to use the more radical cutoff

$$\mathcal{O}(\alpha) \geq \begin{cases} 2n_p & \text{if } n_l = 0 , \\ n_l & \text{if } n_p = 0 , \\ 2n_p + n_l + 1 & \text{otherwise} , \end{cases} \tag{13}$$

which we admit is still not optimal. Second, we note that it is sufficient to reduce the list of clusters to those which are topologically inequivalent. Clusters are topologically equivalent if they can be transformed into one another by deformations and reflections which do not make breaks or joins between links, such as in Fig. 3. To see that this reduced list is sufficient, define $U_l' = \eta_l U_l$ in the Hamiltonian (1) and note that η_l and U_l can be eliminated from (1d) and (1e) in favor of U_l'. [The product of η_l's around any plaquette is -1, so (1e) loses its minus sign.] Topological deformations of clusters leave plaquettes intact, and therefore leave $E_\alpha^{(2N)}$ invariant. The embedding and lattice constants must of course now count embeddings which involve topological deformations.

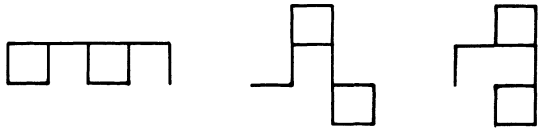

FIG. 3. Topologically equivalent clusters with $n_p = 2$, $n_l = 3$.

B. Chiral condensate

We next consider the strong-coupling series expansion for the chiral condensate per lattice site, defined by

$$\langle \bar{\psi}\psi \rangle^{\text{lattice}} = \frac{1}{2N_s} \sum_r (-1)^{r_1 + r_2} [\chi^\dagger(r), \chi(r)] , \tag{14}$$

or $\frac{1}{2}$ (average number of fermions per site), since the unperturbed vacuum state $| A \rangle$ contains no fermions. N_s is the number of sites in the lattice. The physical chiral condensate in the continuum limit is related to this quantity by

$$\begin{aligned} \langle \bar{\psi}\psi \rangle^{\text{physical}} &= (2a)^{-2} \langle \bar{\psi}\psi \rangle^{\text{lattice}} \\ &= \tfrac{1}{4} e^4 y^2 \langle \bar{\psi}\psi \rangle^{\text{lattice}} . \end{aligned} \tag{15}$$

The series expansion for $\langle \bar{\psi}\psi \rangle^{\text{lattice}}$ can once again be written in diagrammatic form and the linked cluster method is applicable.

Analogous to Eqs. (10) and (12) we have

$$\langle \bar{\psi}\psi \rangle^{\text{lattice}} = \tfrac{1}{2} - \sum_\alpha l_\alpha \bar{\epsilon}_\alpha^{(2N)}(y) + O(y^{2N+2}) , \tag{16}$$

$$J_\alpha^{(2N)} = \sum_\beta C_\beta^\alpha \bar{\epsilon}_\alpha^{(2N)} . \tag{17}$$

In Eq. (17), $J_\alpha^{(2N)}$ is the series expansion to order $2N$ of

$$\frac{\langle 0,\alpha | J | 0,\alpha \rangle}{\langle 0,\alpha | 0,\alpha \rangle} ,$$

where $| 0,\alpha \rangle$ is the ground state of the Hamiltonian restricted to the cluster α, and J is the operator which counts the number of fermions present (i.e., electrons plus positrons). Writing

$$| 0,\alpha \rangle = | 0 \rangle + y | 1 \rangle + y^2 | 2 \rangle + \cdots ,$$

$$J_\alpha^{(2N)} = \sum_{n=1}^{N} j_{2n} y^{2n} ,$$

we have

$$j_{2n}=\frac{2\sum_{k=0}^{n-1}\langle k\mid J\mid 2n-k\rangle+\langle n\mid J\mid n\rangle}{2\sum_{k=0}^{n-1}\langle k\mid 2n-k\rangle+\langle n\mid n\rangle}\ . \tag{18}$$

The algorithm from Ref. 17 used to evaluate $E_\alpha^{(2N)}$ in the ground-state energy calculation involves an iterative evaluation of $|0,\alpha\rangle$ only to order y^n in terms of the strong-coupling basis. However, J is diagonal in the strong-coupling basis, and the iterative procedure can be extended to produce the required components of $|n+1\rangle, |n+2\rangle,\ldots, |2n\rangle$ without generating extra strong-coupling basis states. The matrix elements in (18) can then be evaluated, and finally (16) and (17) are used to generate the required series expansion for $\langle\bar\psi\psi\rangle^{\text{lattice}}$.

C. Mass gaps

A somewhat trickier expansion for handling mass gaps involving disconnected clusters is described in Refs. 18 and 5. The presence of first- and second-order perturbations in our Hamiltonian causes no serious new problems, and the arguments set out in Sec. 3.1 of Ref. 18 apply, without modification, to the perturbation $V=yW_1+y^2W_2$. We have evaluated series expansions for the masses m_S and m_A of the symmetric and antisymmetric pure gauge states whose unperturbed eigenstate forms are

$$\sum_p (U_{\partial p}\pm U_{\partial p}^\dagger)\mid A\rangle\ . \tag{19}$$

Series expansions to order y^{2N} require a set of disconnected clusters to order N. Defining the order of a cluster in this context is more complicated than for the ground-state energy, though we found it adequate to use

$$\mathcal{O}^{(\text{discon})}(\alpha)=\sum_{\substack{\text{connected}\\ \text{components }\beta}}\mathcal{O}(\beta)\ ,$$

where $\mathcal{O}(\beta)$ satisfies the inequality (11). Once again it is sufficient to consider only topologically inequivalent clusters. Any particular diagram in the mass gap series expansion starts and ends with a single plaquette of flux, and introducing once again the link operators $U_l'=\eta_l U_l$, it is clear that the value of the diagram is unaltered by deformation of the cluster it spans.

We have not evaluated series expansions for mesonlike states, i.e., those with a generic unperturbed eigenstate of the form

$$\sum_{r,i}\rho_i(r)\eta_i(r)[\chi^\dagger(r)U_i(r)\chi(r+a\hat i)\pm\text{H.c.}]\mid A\rangle\ .$$

We note in passing, however, that the link-dependent ρ factors distinguishing states with different symmetry properties cause extra problems. A typical diagram will include a factor $\rho_i^*\rho_f$ to take account of the links occupied by the initial and final states, and this factor may feel the effects, not only of topological deformations of clusters, but also rotations and translations. This will extend considerably the list of independent clusters needed at each order.

IV. SERIES RESULTS AND ANALYSIS

We have employed Padé and Shafer approximants[19,5] to analytically continue our strong-coupling expansions past their radius of convergence, towards the physically meaningful weak-coupling regime. The $[N/M]$ Padé approximant $f_{[N/M]}(z)$ to a function $f(z)$ is defined in terms of the polynomials $P_N(z)$ and $Q_M(z)$, of order N and M, respectively, satisfying

$$Q_M(z)f(z)-P_N(z)=O(z^{N+M+1}),\quad Q_M(0)=1\ ,$$

as

$$f_{[N/M]}(z)=\frac{P_N(z)}{Q_M(z)}\ .$$

The $[p/q/r]$ Shafer approximant to $f(z)$ is similarly defined in terms of polynomials $P(z)$, $Q(z)$, and $R(z)$ of order p, q, and r satisfying

$$P(z)f^2(z)+Q(z)f(z)+R(z)=O(z^{p+q+r+2})\ ,$$

$$P(0)=1\ ,$$

as

$$f_{[p/q/r]}(z)=\frac{-Q(z)\pm[Q^2(z)-4P(z)R(z)]^{1/2}}{2P(z)}\ .$$

In general, one believes that series approximants will better approximate the global analytic structure of the function in question than the original truncated series expansion. For instance, Shafer approximants are better able to approximate square-root singularities which may be present in the complex plane. In our analysis we have calculated diagonal and near diagonal Padé and Shafer approximants to the highest available orders and assume that these give an accurate analytical continuation in the range over which they agree. In all cases below, the Padé and Shafer approximants are calculated from series expansions in the variable y^2, so that an $[N/M]$ Padé approximant, for instance, is calculated from a series expansion to $O(y^{2(N+M)})$.

Table I shows series-expansion coefficients to order y^{16} (or $N=8$) for the ground-state energy per site ω_0 and chiral condensate $\langle\bar\psi\psi\rangle^{\text{lattice}}$ at $\mu=0.0$, 0.3, 0.5, and 2.0. Generation of clusters to this order and determination of embedding constants took approximately 15 h of VAX 11/780 CPU time, while calculating the series expansions took an initial 7 h to generate the Fock-space basis states plus a further 6 h CPU time for each value of μ. These times increase by a factor of about 10 for each order in y^2.

For small μ, the coefficients oscillate in sign and grow rapidly in magnitude with increasing order. This behavior can be traced to a pole on the negative y^2 axis near the origin. Padé analysis of the logarithmic derivative[20] of the specific heat[21] $x^2(d^2\omega_0/dx^2)$, where $x=y^2$, reveals a pole in the specific heat at $x_c\approx-0.026$ when $\mu=0$. This pole moves out along the negative x axis as μ increases, and approaches the origin as $\mu\to-\frac{1}{2}$, at

TABLE I. Coefficients of y^{2N} in strong-coupling series expansions of the ground-state energy ω_0 and chiral condensate $\langle\bar{\psi}\psi\rangle^{\text{lattice}}$

N \ μ	0.0	0.3	0.5	2.0
		Vacuum energy		
1	−2	−1.25	−1	−0.4
2	13.5	2.917 968 75	1.25	−0.388
3	−225.809 523 809 52	−22.396 199 187 340	−7.5625	−0.105 716 363 636 36
4	4740.493 349 632	189.079 301 861 7	41.681 901 041 666 7	0.144 041 348 151 27
5	−114 533.212 040 4	−1837.104 137 250	−264.139 377 467 47	−0.119 637 218 016 7
6	3 019 112.271 99	19 480.975 330 8	1828.909 211 780	0.152 872 543 487 3
7	−84 460 458.641	−219 229.954 97	−13 439.617 345 3	−0.214 626 482 088
8	2 467 210 478	2 575 975.521	103 118.307 24	0.307 575 436 66
		Chiral condensate		
0	0.5	0.5	0.5	0.5
1	−4	−1.5625	−1	−0.16
2	84	12.817 382 812 5	5.25	0.1344
3	−2231.056 689 342 40	−136.790 952 483 222	−36.617 187 5	−0.185 604 533 648 17
4	65 341.586 385 919	1609.059 360 914 92	280.949 001 736 111	0.263 245 277 851 37
5	−2 025 737.847 176 5	−20 049.480 611 731	−2284.382 049 422 6	−0.392 104 857 244 5
6	65 182 947.676 79	259 376.164 876 1	19 290.131 015 10	0.616 529 824 917 6
7	−2 153 203 741.63	−3 445 179.746 68	−167 267.625 734 6	−0.997 819 596 80
8	72 529 772 978	46 665 251.05	1 479 158.2050	1.648 612 396 8

which point the lightest unperturbed mesonlike state becomes degenerate with the unperturbed vacuum. We have been unable to find any singular behavior in the specific heat in the physical region $y^2 > 0$ and assume the theory remains analytic out to the continuum limit $y \to \infty$.

We list in Table II estimates of the quantities ω_0 and $\langle\bar{\psi}\psi\rangle^{\text{lattice}}$ obtained by fitting Padé and Shafer approximants to the strong-coupling series. Approximants to ω_0 for the case $\mu = 0.5$ together with examples of the weak-coupling curve (A9) are plotted in Fig. 4. The transition to weak coupling seems to take place between $y = 1.0$ and 1.5, which is outside the region of convergence of the series approximants. A qualitatively similar picture is obtained for other values of μ, with the transition to weak coupling moving to higher values of y as μ increases, but always remaining just outside the region of convergence of the Padé and Shafer approximants. At

TABLE II. Estimates of vacuum energy per site ω_0 and chiral condensate $\langle\bar{\psi}\psi\rangle^{\text{lattice}}$ as functions of y at $\mu = 0.0$, 0.3, 0.5, and 2.0. Estimated errors in the final figures are given in parentheses.

y \ μ	0.0	0.3	0.5	2.0
		Vacuum energy		
0.2	−0.066 527	−0.046 413	−0.038 399	−0.016 627
0.4	−0.2117(2)	−0.1668(2)	−0.145 06(1)	−0.074 282
0.6	−0.42(1)	−0.34(2)	−0.327(2)	−0.197 30
0.8	−0.69(3)	−0.60(5)	−0.63(2)	−0.4258(1)
1.0	−1.1(5)	−1.0(3)	−1.1(1)	−0.806(2)
1.2			−1.8(4)	−1.36(2)
1.4				−2.0(1)
1.6				−2.9(4)
		Chiral condensate		
0.0	0.5	0.5	0.5	0.5
0.2	0.407 31(1)	0.452 01	0.466 60	0.493 80
0.4	0.312(1)	0.377 56(8)	0.405 63(3)	0.477 22
0.6	0.25(1)	0.3133(10)	0.3472(4)	0.454 06
0.8	0.15(5)	0.25(1)	0.293(3)	0.4268(1)
1.0		0.21(3)	0.24(1)	0.3970(4)
1.2			0.19(3)	0.366(4)
1.4				0.33(1)
1.6				0.31(2)
1.8				0.26(3)

$\mu=0$ we estimate the weak-coupling transition to be between 0.5 and 1.0, and for $\mu=2$ to be between $y=1.4$ and 2.0.

Plots of Padé and Shafer approximants to the chiral condensate for the massless theory are shown in Fig. 5. From the analysis of Pisarski[8] and others[10,14] we expect a nonzero chiral condensate in the continuum limit $y\rightarrow\infty$. If we further assume naive dimensional scaling consistent with Eq. (15), one expects $\langle\bar{\psi}\psi\rangle^{\text{lattice}}\sim ky^{-2}$ for large y. Our strong-coupling series approximants do not converge well enough to exhibit this behavior explicitly, but are not inconsistent with the weak-coupling dashed curve shown, which has $k=0.2$. This corresponds to a physical chiral condensate

$$e^{-4}\langle\bar{\psi}\psi\rangle^{\text{physical}}\simeq 0.05\ . \tag{20}$$

We next turn to the finite mass theory, in which chiral symmetry is explicitly broken. Considering only the pure fermion Hamiltonian, Eq. (5), one can derive an exact expression for the chiral condensate, as outlined in the Appendix. The result is

$$\langle\bar{\psi}\psi\rangle^{\text{lattice}}$$

$$=\frac{\mu}{\pi^2 y}\int_0^{\pi/2}dp\int_0^{\pi/2}dq\left[\cos^2 p+\cos^2 q+\frac{\mu^2}{4y^2}\right]^{-1/2} \tag{21}$$

$$\underset{y\rightarrow\infty}{\sim}\ \text{const}/y\ . \tag{22}$$

The addition of the gauge field in the full theory is only expected to introduce corrections $O(y^{-2})$—see the Appendix. So from Eq. (15) we see that the physical chiral condensate should diverge in the continuum limit for massive fermions, proportionally to y.

In Fig. 6 are plotted series approximants for $y\langle\bar{\psi}\psi\rangle^{\text{lattice}}$ at $\mu=2$, the factor of y being included to exhibit the asymptotic behavior at large y. The lower of the two dashed curves is the pure fermion theory condensate (21). By arbitrarily adding $0.1y^{-2}$ to $\langle\bar{\psi}\psi\rangle_f^{\text{lattice}}$ to allow for the next-order weak-coupling corrections, we obtain a more convincing fit to the strong-coupling curves, the changeover to weak couping occurring once again just outside the reach of the series approximants. Convergence of the series approximant at $\mu=0.3$ and 0.5 is unfortunately somewhat worse, and analogous plots for these cases fail to offer a convincing match with weak-coupling curves.

In Table III we list the strong-coupling series expansions to $O(y^8)$ for the mass gaps m_S and m_A of the photonballs obtained by perturbing the strong-coupling mass eigenstates (19). Evaluation of the required disconnected cluster embedding constants is computationally slow, the CPU time to this order being about 20 h on a VAX 11/780. This CPU time increases by a factor of about 15 for each extra order of y^2. The subsequent calculation of the series expansions took about 1 h of CPU time for each value of μ.

Figure 7 shows the spread of the [1/2], [2/1], and [2/2] Padé and [1/1/1] Shafer approximants to the antisymmetric state mass gap series for several values of μ. Numerical estimates of both m_A and m_S in dimension-

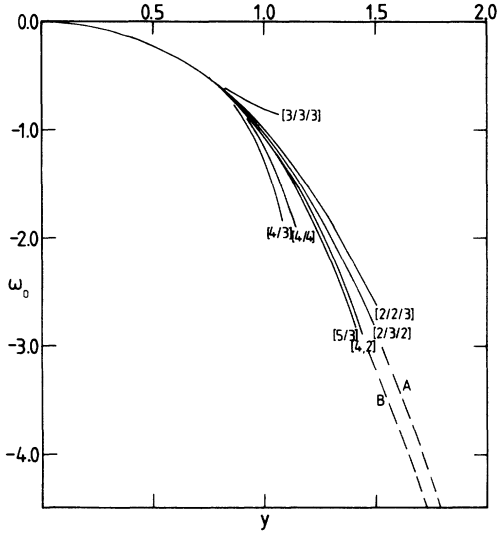

FIG. 4. Series approximants to the ground-state energy ω_0 at $\mu=0.5$. The dashed curves are the $O(1)$ weak-coupling form Eq. (A9); $\omega_0=2y^2+0.9581y+C$ where $C=0.2$ in curve A and $C=-0.2$ in curve B. Padé approximants are labeled $[p/q]$ and Shafer approximants $[p/q/r]$.

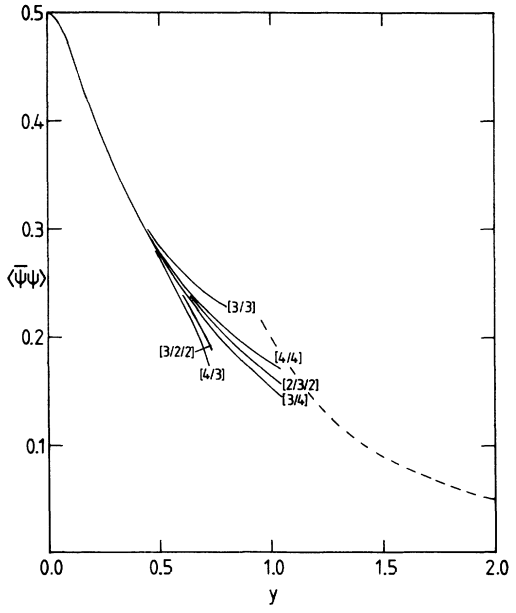

FIG. 5. Graph of series approximants to the chiral condensate $\langle\bar{\psi}\psi\rangle^{\text{lattice}}$ at $\mu=0$, and the weak-coupling fit $0.2y^{-2}$.

less units are listed in Table IV. The approximants fail to converge much past $y=0.5$ in most cases and give little indication of their continuum-limit behavior. From Eqs. (1) and (2) we expect

$$\frac{E^{\text{physical}}}{m}=\frac{\omega_1}{\mu},$$

where E^{physical} is an eigenvalue of the Hamiltonian H in (1) and ω_1 is the corresponding mass gap calculated from the dimensionless Hamiltonian W. At fixed μ we therefore expect the curves in Fig. 7 to become constant in the continuum limit $y\to\infty$.

At $\mu=0$, $\frac{1}{2}$, and $\frac{3}{2}$ there exist mesonlike strong-coupling eigenstates mass degenerate with the pure gauge states (19). Close to these values of μ, singularities near to zero on the negative y^2 axis cause the coefficients to oscillate in sign and grow rapidly in magnitude with increasing order of perturbation. The coefficients become infinite as μ approaches these values. At $\mu_C=0$ and $\frac{3}{2}$ there seems to be no particular problem, at least to order y^8, in approaching the limit $\mu\to\mu_C$ from above or below. Calculations at $\mu=\pm0.01$, for in-

TABLE III. Coefficients of y^{2N} in the strong-coupling series expansions of the antisymmetric and symmetric photon-ball mass gaps m_A and m_S of the dimensionless Hamiltonian W.

μ	N	Antisymmetric state	Symmetric state
−0.01	0	4.0	4.0
	1	5.371 276 027 189 40	5.371 276 027 189 40
	2	−45.898 824 904 633	−44.732 158 237 966
	3	1001.907 620 040	989.867 945 340 9
	4	−23 566.584 449 2	−23 298.944 008 0
0.01	0	4.0	4.0
	1	5.300 133 298 352 45	5.300 133 298 352 45
	2	−40.439 926 334 044	−39.273 259 667 377
	3	822.428 509 055 6	810.465 043 629 0
	4	−21 513.425 812 2	−21 278.811 256 5
0.1	0	4.0	4.0
	1	5.206 333 333 333 33	5.208 333 333 333 33
	2	−23.567 292 390 046	−22.400 625 723 380
	3	368.489 225 438 0	354.283 857 961 1
	4	−6414.418 696 77	−6258.332 010 30
0.4	0	4.0	4.0
	1	11.695 906 432 748 5	11.695 906 432 748 5
	2	−134.437 726 877 92	−133.271 060 211 26
	3	5645.960 797 986	4172.876 167 315
	4	−308 460.430 890	−157 304.631 067
0.6	0	4.0	4.0
	1	−8.658 008 658 008 66	−8.658 008 658 008 66
	2	369.027 983 474 64	370.194 650 141 31
	3	−22 591.681 729 48	−23 538.725 234 72
	4	1 646 709.672 02	1 848 123.710 904
0.8	0	4.0	4.0
	1	−2.229 654 403 45	−2.229 654 403 567 45
	2	18.845 653 555 031	20.012 320 221 698
	3	−212.456 655 306 3	−210.621 782 708 4
	4	2408.879 749 86	2567.634 462 35
1.6	0	4.0	4.0
	1	−0.279 290 601 871 25	−0.279 290 601 871 25
	2	−1.078 016 175 469 4	8.865 049 119 721 8E-02
	3	−1.184 612 894 106	−3.723 629 359 264
	4	3.801 587 760 64	60.545 334 540 6
2.0	0	4.0	4.0
	1	−0.152 380 952 380 95	−0.152 380 952 380 95
	2	−1.401 913 616 240 2	−0.235 246 949 573 5
	3	−0.347 320 851 264	−0.489 055 293 189
	4	1.695 152 914 87	2.073 466 005 65
2.4	0	4.0	4.0
	1	−9.307 087 347 014 74E-02	−9.307 087 347 014 74E-02
	2	−1.504 104 257 967 9	−0.337 437 591 301 2
	3	−0.143 439 779 690	−0.154 278 244 536
	4	1.323 460 521 64	0.787 266 619 72

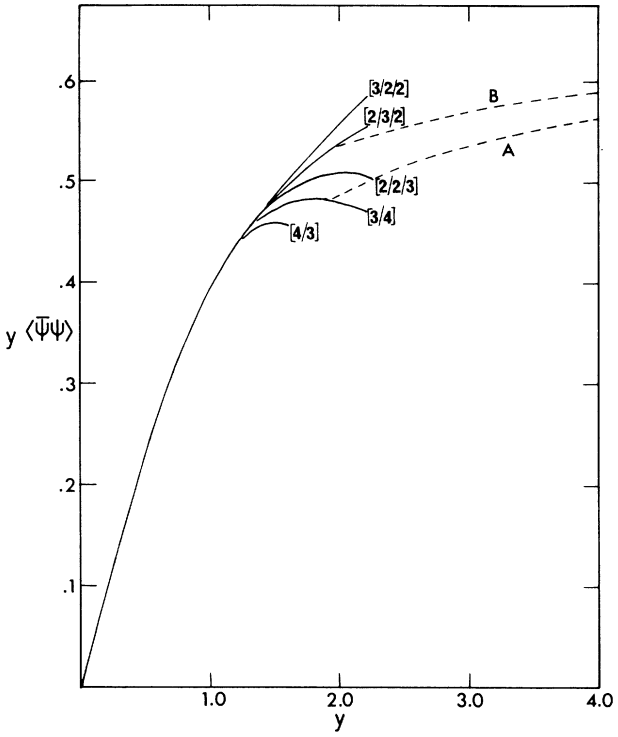

FIG. 6. Graph of $y\langle\bar{\psi}\psi\rangle^{\text{lattice}}$ against y at $\mu=2$, together with curve A the pure fermion case, and curve B the same curve with $0.1y^{-2}$ added to allow for the $O(y^{-2})$ weak-coupling corrections.

stance, give almost identical series approximants. On the other hand, as μ pass through the value $\frac{1}{2}$, we observe a violent jump in the behavior of the mass gaps. To see what is happening here, consider an effective two-state Hamiltonian restricted to the relevant pure gauge and mesonlike states:

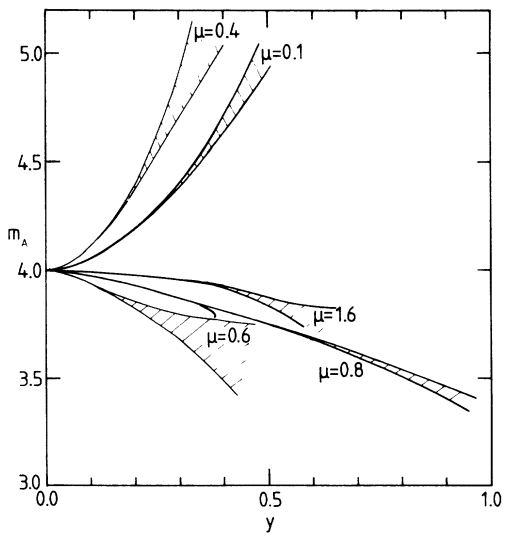

FIG. 7. Graphs of the antisymmetric photon-ball mass gap m_A (eigenvalues of the dimensionless Hamiltonian W), for various values of μ. The shaded areas exhibit the spread of the [1/2], [2/1], and [2/2] Padé and [1/1/1] Shafer approximants excluding obvious outliers.

$$H=\begin{pmatrix} 4 & ky \\ ky & 3+2\mu \end{pmatrix}$$

with some arbitrary coupling k between the states. Setting $\epsilon=\mu-\frac{1}{2}$, the mass eigenstates are

$$\omega_1^{\pm}=4+\epsilon\pm(\epsilon^2+k^2y^2)^{1/2}\ .$$

As ϵ passes through zero, the eigenvalue relevant to the pure gauge state jumps from the negative square root to the positive square root. This level-crossing phenomenon is a lattice artifact and has nothing to do with the continuum limit. Although the upward tendency of the mass gap curves for $\mu<\frac{1}{2}$ may indicate a high photon-ball mass for small μ in the continuum limit, the erratic behavior of the curves around $\mu=\frac{1}{2}$ precludes a definite interpretation.

Finally we compare mass differences between the symmetric and antisymmetric photon-balls, a few examples being plotted in Fig. 8. For $\mu\lesssim\frac{1}{2}$ series approximants for the two states give almost identical results. The behavior at small y values is principally driven by the strong-coupling mass degeneracy at $\mu=\frac{1}{2}$, and we believe no reliable conclusions can be drawn about m_S/m_A in the continuum limit. For $\mu\gtrsim0.8$ the curves begin to show definite splitting between the symmetric and antisymmetric states indicating that the symmetric state is more massive, and that a rapid falloff in mass sets in at larger y. This is to be expected since in the limit $\mu\to\infty$ the glueball spectrum will decouple and behave as in the pure gauge theory, where $m_S/m_A=2$ in the continuum limit, and the glueball mass drops exponentially at large y (Refs. 22 and 5).

Before completing this section, we mention that Horn *et al.*,[23] found it advantageous to fit Padé approximants to derivatives of functions, rather than the original functions, when dealing with their t expansions. We tried similar techniques for the chiral condensate curves above, [e.g., fitting Padé approximants to $d\langle\bar{\psi}\psi\rangle^{\text{lattice}}/d(y^2)$ and then integrating], but found no significant improvement in the domain of convergence of the series approximants.

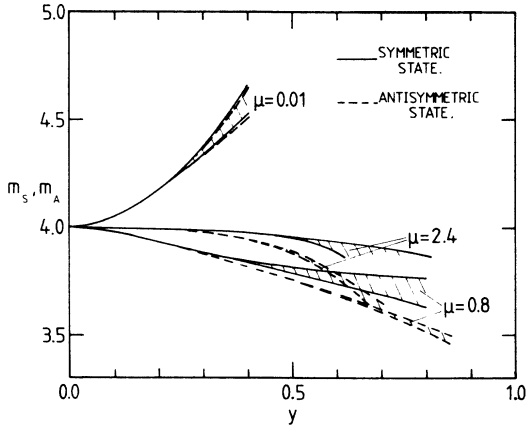

FIG. 8. The same as Fig. 7 for both the symmetric and antisymmetric photon-ball mass gaps.

TABLE IV. Estimates of antisymmetric and symmetric photon-ball mass gaps m_A and m_S as functions of y. Estimated errors in the final figures are given in parentheses.

y \ μ	0.01		0.1		0.4	
	A	S	A	S	A	S
0.1	4.0496	4.0497	4.0500(1)	4.0500(1)	4.1074(2)	4.1068
0.2	4.175(2)	4.177(3)	4.185(1)	4.186(1)	4.38(2)	4.37(2)
0.3	4.34(2)	4.36(2)	4.39(1)	4.39(1)	4.8(1)	4.75(8)
0.4	4.58(8)	4.59(7)	4.67(4)	4.68(4)	5.4(5)	5.3(3)
0.5	4.8(2)	4.9(2)	5.0(1)	5.1(2)	6(1)	6(1)
0.6	5.2(4)	5.2(4)	5.6(4)	5.6(4)		
0.7	5.6(9)	5.8(8)	6.3(6)	6.3(7)		
y \ μ	0.6		0.8		2.4	
	A	S	A	S	A	S
0.1	3.9367(4)	3.9365(5)	3.9794	3.9795	3.9989	3.9990
0.2	3.84(1)	3.84(2)	3.9316	3.9335(2)	3.9937(1)	3.9957
0.3	3.73(6)	3.73(7)	3.8752(1)	3.884(2)	3.9793(1)	3.9888
0.4	3.6(2)	3.6(2)	3.8159(6)	3.840(6)	3.9465(5)	3.9760(5)
0.5	3.5(3)	3.4(4)	3.753(2)	3.80(2)	3.883(3)	3.953(4)
0.7			3.61(1)	3.73(5)	3.60(4)	3.8(2)
0.8			3.52(2)	3.70(8)	3.4(1)	
0.9			3.44(4)	3.7(1)	3.0(3)	

V. POSSIBLE IMPROVEMENTS WITH EXACT TERMS

It is important to estimate the likely improvements to the series extrapolations as extra terms are added to our series. With this knowledge, we can critically evaluate the future usefulness of our method in dealing with dynamical fermions. As an example, we examine the effect on our chiral condensate results for the massless theory when the last few terms in the strong-coupling series are truncated.

Figure 9 shows the highest order available $[N/N+1]$, $[N/N]$, and $[N-1/N]$ Padé approximants to the chiral condensate series taken to order y^8, y^{12}, and y^{16}. If we arbitrarily decide that a variation of 2% either side of the mean of the $[N/N-1]$, $[N/N]$, and $[N-1/N]$ approximants is tolerable, then the truncated series converge out to the points indicated by the arrows. For series to $O(y^8)$, $O(y^{12})$, and $O(y^{16})$, we have reliable results out to $y=0.28$, 0.42, and 0.54, respectively.

A rough extrapolation of these figures indicates that a series of $O(y^{24})$ may converge out to about $y=0.75$ or 0.8, which is perhaps far enough to begin making serious quantitative predictions about the matching to the weak-coupling behavior (see, for example, Fig. 5). This would require an extra four terms of the series expansion, or, without significant changes to the computer codes, an increase by a factor of 10^4 in CPU time. A certain amount of streamlining is further possible in the computer codes by removing unnecessary clusters from the cluster list, and by avoiding unnecessary strong-coupling basis states in the individual cluster perturbation expansions. It is difficult to say whether or not the resulting calculation would be accessible to a supercomputer.

If we examine Fig. 9 further, we see evidence that the $[N-1/N]$ Padé approximants are converging more rapidly than the other Padé approximants as N increases, the [2/3] and [3/4] approximants agreeing to within 4% out to $y=0.7$. Recalling that the Padé approximants are calculated as rational functions of y^2, we see this as

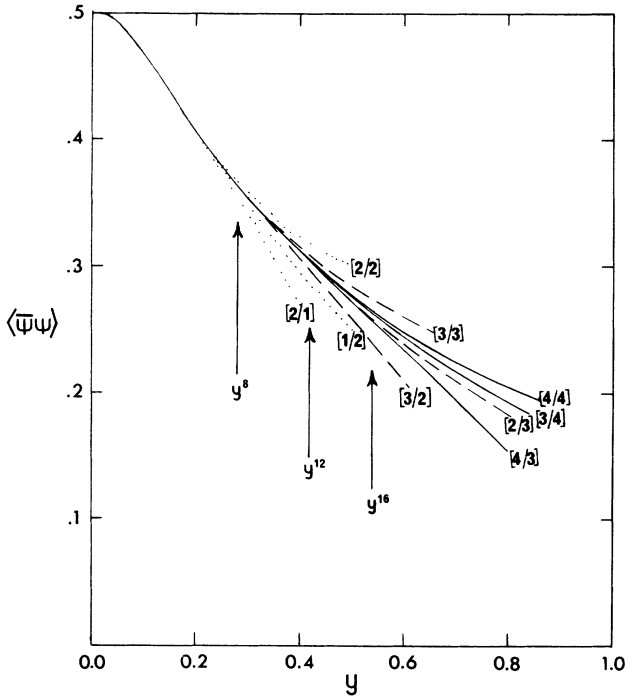

FIG. 9. The $[N/N-1]$, $[N/N]$, and $[N-1/N]$ Padé approximants to $\langle\bar{\psi}\psi\rangle^{\text{lattice}}$ calculated from strong-coupling series expansions to $O(y^8)$ (dotted curve), $O(y^{12})$ (dashed curve), and $O(y^{16})$ (solid curve). The arrows indicate approximately the values of y at which the three approximants at each order differ from their mean by $\pm 2\%$.

evidence for the assumed asymptotic behavior $\langle \bar{\psi}\psi \rangle^{\text{lattice}} \sim ky^2$ as $y \to \infty$. As more terms are added to the series, it will become apparent whether the convergence of the [2/3] and [3/4] Padé approximants is fortuitous, or continues to hold for higher $[N-1/N]$ Padé approximants, in which case two more $[N-1/N]$ Padé approximants could well be sufficient to match the weak-coupling behavior. This would require only three extra terms in the strong-coupling series, which could well be a feasible project for a supercomputer.

Similar predictions should hold for the vacuum energy and massive chiral condensate series. The outlook is considerably less promising, however, for the photon-ball mass gap series, which still have a long way to go before any quantitatively useful results emerge. While we have not attempted mass gap calculations for meson-like states, it is unlikely that cluster expansions for these would do significantly better.

VI. CONCLUSIONS

As a first attempt at applying linked cluster expansions to a gauge theory with fermions we have used the method to study $(2+1)$-dimensional quantum electrodynamics. Hamiltonian strong-coupling expansions of the ground-state energy and chiral condensate to $O(y^{16})$ [or $O(g^{-32})$ in terms of the dimensionless coupling] have been generated numerically for various fermion masses. Extrapolations towards weak coupling using Padé and Shafer approximants fall short of an accurate quantitative matching onto weak-coupling expansions, though the correct qualitative behavior has been observed. Our rough estimate of the dynamically generated chiral condensate is given by (20). Convergence of the series approximants is worst for small fermion mass μ, where the series coefficients feel the effects of a singularity close to the origin on the negative y^2 axis, caused by an unphysical vacuum degeneracy in the strong-coupling limit at $\mu = -\frac{1}{2}$.

Strong-coupling expansions of the antisymmetric and symmetric photon-ball mass gaps have also been generated, but only to $O(y^8)$ (or g^{-16}). Convergence of the Padé and Shafer approximants is poor, partly due to a mass degeneracy in the strong-coupling limit at $\mu = \frac{1}{2}$, and it is difficult to draw confident conclusions about the continuum limit. The inequality $m_S > m_A$ seems to hold at least for $\mu > 0.8$, and there is evidence to suggest a photon-ball mass large compared with the bare electron mass for $\mu < 0.5$.

The strong-coupling expansion technique has previously been applied to the pure U(1) gauge theory with good results.[5] In the present theory, we have found that the case with the dynamical fermions is much more difficult. According to our analysis in Sec. V, it is conceivable that the vacuum energy and chiral condensate expansions could be extended far enough to reach the weak-coupling region using a supercomputer. One drawback of the cluster expansion method, as with most numerical lattice calculations, is that the calculation only spans a finite number of lattice spacings. However, an accurate determination of nonperturbative chiral symmetry breaking, for instance, requires consideration of large fermion loops. Our chiral condensate calculations have included fermion loops spanning up to 8 lattice spacings, while our estimates of Sec. V suggest that calculations involving diagrams up to 11 or 12 lattice spacings may be sufficient to provide a reasonable matching onto weak-coupling behavior. This may be compared with recent finite-temperature Monte Carlo simulations[24] on lattices stretching to 8 or 10 spatial lattice sites, which report asymptotic scaling violations at the couplings relevant to these lattice sizes. The problem of long-distance effects is of course more pronounced for the mass gaps, which depend on the rate of falloff of long-range correlations. It is unlikely that our mass gap series expansions could be extended far enough to provide useful results in the foreseeable future.

It is clear that further technical developments will be necessary before Hamiltonian strong-coupling expansions can compete favorably with Monte Carlo algorithms in the treatment of theories with dynamical fermions. This is particularly so for the current problem, and for QCD, both of which only become physically interesting in the weak-coupling limit. We have also recently completed a more successful analysis of $(3+1)$-dimensional QED, for which a phase transition at finite coupling is expected. Details of this calculation will be given elsewhere.[25]

Finally, we note the existence of alternate numerical algorithms for studying Hamiltonian lattice gauge theory, such as the t expansion,[23] and the use of variational wave functions,[26] both of which have produced good results for pure gauge theories. We are unaware of any attempt to apply these methods to theories with dynamical fermions, but feel that the results of the current investigation could provide a useful check on the strong-coupling regime of subsequent lattice Hamiltonian calculations with fermions.

ACKNOWLEDGMENTS

We would like to thank A. N. Burkitt, A. C. Irving, and M. N. Barber for helpful discussions. While completing this paper we received a paper describing a Monte Carlo analysis of Euclidean three-dimensional QED with dynamical fermions by Irving and Burkitt.[27]

APPENDIX: WEAK-COUPLING EXPANSIONS FOR (2+1)-DIMENSIONAL QED

We extend the pure gauge theory weak-coupling expansion of Hofsäss and Horsley[28] to include fermions. Writing $U_l = \exp(iy^{-1/2}\theta_l)$, The Hamiltonian (1) can be written

$$\frac{W}{y}=\mathcal{H}^g+\left[\sum_l \eta_l[(\chi^\dagger\chi)_l+\text{H.c.}]+\frac{\mu}{y}\sum_r(-1)^r\chi^\dagger(r)\chi(r)\right]$$
$$+iy^{-1/2}\sum_l \eta_l[(\chi^\dagger\chi)_l-\text{H.c.}]\theta_l-\tfrac{1}{2}y^{-1}\sum_l \eta_l[(\chi^\dagger\chi)_l+\text{H.c.}]\theta_l{}^2+O(y^{-3/2})$$
$$=\mathcal{H}^g+\mathcal{H}_0^f+y^{-1/2}\mathcal{H}_{1/2}^f+y^{-1}\mathcal{H}_1^f+\cdots\ . \tag{A1}$$

In (A1), $\mathcal{H}^g$ contains contributions from the pure gauge parts W_e and W_2. The analysis of Ref. 29 gives the ground-state energy per site of $y\mathcal{H}^g$ as

$$\omega_0^g=-2y^2+1.9162y+O(1) \tag{A2}$$

with eigenvector

$$|D\rangle=\exp\left[-\tfrac{1}{2}\sum_{l,l'}\theta_l D_{ll'}^{1/2}\theta_l\right]+O\left[\frac{1}{y}\right]; \tag{A3}$$

details of the matrix D being given in Ref. 28.

To determine the ground-state eigenvalue of $\mathcal{H}_0^f$, define Fourier-transformed fermion fields ζ_j by

$$\chi_j(r)=\left[\frac{4}{N_S}\right]^{1/2}\sum_q e^{i(q_1r_1+q_2r_2)}\zeta_j(q)\ ,$$
$$q_{1,2}=\frac{\pi}{M},\frac{3\pi}{M},\ldots,\frac{(M-1)\pi}{M}\ , \tag{A4}$$

where $\chi_j;j=1,2,3,4$ is the value of χ on each of the four sublattices in Fig. 1 and $N_S=M^2$ (M even) is the number of sites in the finite lattice. A straightforward calculation gives

$$\mathcal{H}_0^f=2\sum_q(\{[-\zeta_1^\dagger(q)\zeta_2(q)+\zeta_4^\dagger(q)\zeta_3(q)]\cos q_x+[\zeta_1^\dagger(q)\zeta_4(q)+\zeta_2^\dagger(q)\zeta_3(q)]\cos q_y\}+\text{H.c.})$$
$$+\frac{\mu}{y}\sum_q[\zeta_1^\dagger(q)\zeta_1(q)-\zeta_2^\dagger(q)\zeta_2(q)+\zeta_3^\dagger(q)-\zeta_4^\dagger(q)\zeta_4(q)]$$
$$\equiv\sum_q h(q)\ . \tag{A5}$$

The operator $h(q)$ acts on a 16-dimensional Fock space spanned by $|0\rangle$, $\Phi_k=\zeta_k^\dagger(q)|0\rangle$, $\Phi_{jk}=\zeta_j^\dagger\zeta_k^\dagger|0\rangle$, etc. The vacuum is a "Fermi sea" with half the fermion states filled (those with negative energy), and resides in the 2-particle subspace spanned by the ordered basis $\{\Phi_{13},\Phi_{12},\Phi_{43},\Phi_{14},\Phi_{23},\Phi_{24}\}$, where $h(q)$ is represented by the matrix

$$h(q)=\begin{bmatrix}2\rho & Y & Y & X & -X & 0\\ Y & 0 & & & & -Y\\ Y & & 0 & & & -Y\\ X & & & 0 & & -X\\ -X & & & & 0 & X\\ 0 & -Y & -Y & -X & X & -2\rho\end{bmatrix},\quad \rho=\frac{\mu}{y},\quad X=2\cos q_1,\quad Y=2\cos q_2\ . \tag{A6}$$

The minimal eigenvalue and eigenstate are

$$\lambda_0=-2(X^2+Y^2+\rho^2)^{1/2},\quad |\Psi_0\rangle=2\sqrt{}(\rho+\sqrt{})\begin{bmatrix}-(X^2+Y^2)\\ Y(\rho+\sqrt{})\\ Y(\rho+\sqrt{})\\ X(\rho+\sqrt{})\\ -X(\rho+\sqrt{})\\ (\rho+\sqrt{})^2\end{bmatrix}, \tag{A7}$$

where

$$\sqrt{}\equiv(X^2+Y^2+\rho^2)^{1/2}\ .$$

Summing $\langle\Psi_0|\lambda_0|\Psi_0\rangle$ over momenta and taking the continuum limit [i.e., $\Sigma_q\to(4\pi^2)^{-1}N\int_0^\pi dq_0\int_0^\pi dq_2$], gives the ground-state energy per site of $y\mathcal{H}_0^f$ as

$$\omega_0^f = -\frac{4y}{\pi^2}\int_0^{\pi/2} dq_1 \int_0^{\pi/2} dq_2 \left[\cos^2 q_1 + \cos^2 q_2 + \frac{\mu^2}{4y^2}\right]^{1/2} . \tag{A8}$$

Adding (A2) and the piece of (A8) proportional to y gives, after a numerical integration, the weak-coupling limit of the ground-state energy per site:

$$\omega_0(y) = -2y^2 + 0.9581y + O(1) . \tag{A9}$$

The ground-state expectation value of the chiral condensate per site for the pure fermion Hamiltonian $\mathcal{H}_0^f$ is

$$\begin{aligned}\langle \bar{\psi}\psi \rangle_f^{\text{lattice}} &= \sum_q \langle \psi_0 \mid \xi_1^\dagger \xi_1 - \xi_2^\dagger \xi_2 + \xi_3^\dagger \xi_3 - \xi_4^\dagger \xi_4 \mid \psi_0 \rangle \\ &= \frac{\mu}{\pi^2 y}\int_0^{\pi/2} dq_1 \int_0^{\pi/2} dq_2 \left[\cos^2 q_1 + \cos^2 q_2 + \frac{\mu^2}{4y^2}\right]^{-1/2} .\end{aligned} \tag{A10}$$

We claim that (A10) also gives the chiral condensate $\langle \bar{\psi}\psi \rangle^{\text{lattice}}$, correct to order y^{-1}, for the full Hamiltonian (A1), that is

$$\langle \bar{\psi}\psi \rangle^{\text{lattice}} = \langle \bar{\psi}\psi \rangle_f^{\text{lattice}} + O(y^{-2}) . \tag{A11}$$

To see this, consider a Rayleigh-Schrödinger perturbation expansion for (A1) with $\mathcal{H}^g + \mathcal{H}_0^f$ as the unperturbed Hamiltonian. Write the ground state

$$\mid \text{GS} \rangle = \mid 0 \rangle + y^{-1/2} \mid 1 \rangle + y^{-1} \mid 2 \rangle + \cdots$$

with $\mid 0 \rangle = \mid D \rangle \otimes \mid Q \rangle$, where $\mid D \rangle$ is given by (A3) and $\mid Q \rangle$ is the ground state of $\mathcal{H}_0^f$. Then

$$\langle \text{GS} \mid \bar{\psi}\psi \mid \text{GS} \rangle = \frac{\langle 0 \mid \bar{\psi}\psi \mid 0 \rangle + y^{-1}(2\langle 0 \mid \bar{\psi}\psi \mid 2 \rangle + \langle 1 \mid \bar{\psi}\psi \mid 1 \rangle)}{\langle 0 \mid 0 \rangle + y^{-1}(2\langle 0 \mid 2 \rangle + \langle 1 \mid 1 \rangle)} + O(y^{-2}) . \tag{A12}$$

[Note that the $y^{-1/2}$ terms are absent from (A12) because they contain a factor $\langle D \mid \theta_l \mid D \rangle = 0$.] A straightforward perturbation expansion yields the results

$$\begin{aligned}\langle 0 \mid \bar{\psi}\psi \mid 2 \rangle &= \langle 0 \mid \bar{\psi}\psi \mid 2 \rangle_{\text{fermion part}} \langle D \mid \theta_l^2 \mid D \rangle , \\ \langle 1 \mid \bar{\psi}\psi \mid 1 \rangle &= \langle 1 \mid \bar{\psi}\psi \mid 1 \rangle_{\text{fermion part}} \langle D \mid \theta_l^2 \mid D \rangle ,\end{aligned} \tag{A13}$$

where the terms $\langle\ \rangle_{\text{fermion part}}$ are the corresponding terms appearing in a perturbation expansion of the Hamiltonian

$$\mathcal{H}_0^f + iy^{-1/2}\sum_l \eta_l [(\chi^\dagger \chi)_l - \text{H.c.}] - \tfrac{1}{2} y^{-1} \sum_l [(\chi^\dagger \chi)_l + \text{H.c.}] + \cdots . \tag{A14}$$

The θ-dependent factors in (A13) can be accounted for by rescaling $y^{-1/2} \to \Theta y^{-1/2}$, $\Theta = \langle D \mid \theta_l^2 \mid D \rangle$, in (A14). For the purposes of calculating the chiral condensate to $O(Y^{-1})$ it is therefore sufficient to consider the effective Hamiltonian

$$\mathcal{H}_{\text{eff}} = \frac{\mu}{y}\sum_r (-1)^r \chi^\dagger(r)\chi(r) + \sum_l \eta_l [(\chi^\dagger \chi)_l e^{i\Theta/y^{1/2}} + \text{H.c.}] + O(y^{-3/2}) . \tag{A15}$$

Introducing Fourier-transformed fields yields once again the matrix (A6), but this time with

$$x = 2\cos(q_1 + y^{-1}\Theta), \quad Y = 2\cos(q_2 + y^{-1}\Theta) .$$

The calculation proceeds as before, requiring only the change of variables $q_{1,2} \to q'_{1,2} = q_{1,2} + y^{-1}\Theta$ in the last line to recover the form (A8). We note that the equality between $\langle \bar{\psi}\psi \rangle^{\text{lattice}}$ and $\langle \bar{\psi}\psi \rangle_f^{\text{lattice}}$ breaks down at $O(y^{-2})$ because of a mixture of terms containing $\langle D \mid \theta_l^2 \mid D \rangle^2$ and $\langle D \mid \theta_l^4 \mid D \rangle$ prevents factorization similar to (A13) at the next order.

Finally, we comment briefly on the analogous calculation for quantum electrodynamics in (1 + 1) dimensions, i.e., the massive Schwinger model. Assuming the Kogut-Susskind lattice formulation,[1] a calculation similar to but simpler than the one above gives the result

$$\langle \bar{\psi}\psi \rangle^{\text{physical}} = -\frac{m}{\pi}\int_0^{\pi/2} dq (\sin^2 q + m^2 a^2)^{-1/2} \tag{A16}$$

$$\underset{a \to 0}{\sim} -\frac{m}{\pi}\ln(ma) , \tag{A17}$$

where m is the fermion mass and a the lattice spacing. The chiral condensate thus diverges logarithmically in the continuum limit. This exposes an embarrassing error in Ref. 29, where extrapolations were made assuming a *finite* chiral condensate in the continuum limit, and an extensive table of numerical results was presented for massive fermions. In retrospect, the logarithmic divergence in the massive case is clearly evident in Fig. 6 of Ref. 28.

*Present address: School of Physical Sciences, The Flinders University of South Australia, South Australia 5042.
†Present address: School of Physics, University of New South Wales, P.O. Box 1, Kensington, N.S.W. 2033.

[1]T. Banks, L. Susskind, and J. Kogut, Phys. Rev. D **13**, 1043 (1976).
[2]T. Banks *et al.*, Phys. Rev. D **15**, 1111 (1977).
[3]B. G. Nickel (unpublished); L. G. Marland, J. Phys. A **14**, 2047 (1981).
[4]A. C. Irving and C. J. Hamer, Nucl. Phys. **B230** [FS10], 361 (1984).
[5]C. J. Hamer and A. C. Irving, Z. Phys. C **27**, 145 (1985).
[6]A. C. Irving, T. E. Preece, and C. J. Hamer, Nucl. Phys. **B270** [FS16], 536 (1986); C. J. Hamer, A. C. Irving, and T. E. Preece, *ibid.* **B270** [FS16], 533 (1986).
[7]M. J. Lamont, J. Phys. A **20**, 2615 (1987).
[8]R. D. Pisarski, Phys. Rev. D **29**, 2423 (1984).
[9]C. J. Burden and A. N. Burkitt, Europhys. Lett. **3**, 545 (1987).
[10]T. Appelquist *et al.*, Phys. Rev. Lett. **55**, 1715 (1985); Phys. Rev. D **33**, 3704 (1986).
[11]R. Jackiw and S. Templeton, Phys. Rev. D **23**, 2291 (1981).
[12]G. W. Semenoff, Phys. Rev. Lett. **53**, 2449 (1984).
[13]L. Susskind, Phys. Rev. D **16**, 3031 (1977).
[14]S. Rao and R. Yahalom, Phys. Rev. D **34**, 1194 (1986).
[15]C. Domb, in *Phase Transitions and Critical Phenomena,* edited by C. Domb and M. S. Green (Academic, London, 1974), Vol. 3, p. 1.
[16]J. L. Martin, in *Phase Transitions and Critical Phenomena* (Ref. 15), p. 97.
[17]P. G. Hornby and M. N. Barber, J. Phys. A **18**, 827 (1985).
[18]C. J. Hamer and A. C. Irving, J. Phys. A **17**, 1649 (1984).
[19]A. K. Common, J. Phys. A **15**, 3665 (1982).
[20]D. S. Gaunt and A. J. Guttmann, in *Phase Transitions and Critical Phenomena* (Ref. 15), p. 181.
[21]C. J. Hamer and M. N. Barber, J. Phys. A **14**, 241 (1981).
[22]M. Göpfert and G. Mack, Commun. Math. Phys. **82**, 545 (1982).
[23]D. Horn and M. Weinstein, Phys. Rev. D **30**, 1256 (1984); D. Horn, M. Karliner, and M. Weinstein, *ibid.* **31**, 2589 (1985).
[24]F. Karsch *et al.*, Phys. Lett. B **188**, 353 (1987).
[25]C. J. Burden, Australian National University report 1987 (unpublished).
[26]S. A. Chin, C. Long, and D. Robson, Phys. Rev. Lett. **57**, 2779 (1986).
[27]A. C. Irving and A. N. Burkitt, Liverpool report, 1987 (unpublished).
[28]T. Hofsäss and R. Horsley, Phys. Lett. **123B**, 65 (1983).
[29]C. J. Hamer, J. Kogut, D. P. Crewther, and M. M. Mazzolini, Nucl. Phys. **B208**, 413 (1982); for an erratum, see the Appendix of the present paper.